DOI: 10.13009/EUCASS2025-586
11TH EUROPEAN CONFERENCE FOR AERONAUTICS AND SPACE SCIENCES (EUCASS)

Parametric performance evaluation of the Microwave Electrothermal Thruster using monoatomic propellants

Michele Nava[1†], *Michele Lauriola*[2], *Alessandro Maffini*[2], *Matteo Passoni*[2] *and Filippo Maggi*[1]
[1]*Department of Aerospace Science and Technology, Politecnico di Milano, Via La Masa 34, 20156 Milan, Italy*
[2]*Department of Energy, Politecnico di Milano, Via Lambruschini 4a, 20156 Milan, Italy*
[†]Corresponding author, michele1.nava@polimi.it

Abstract

The MET is an electrothermal thruster which uses a microwave-powered plasma to energize a propellant, and accelerates it through a solid nozzle to produce thrust. This study employs a novel global plasma model to perform parametric simulations of a MET operating on helium and argon, evaluating performance dependency on design parameters such as microwave frequency and nozzle throat radius: higher frequency and smaller throat areas produce higher specific impulses for most of the considered specific power range. This study also analyzes the impact of wall heat losses in the nozzle, which appear to produce only a small reduction in the specific impulse at the considered conditions.

1. Introduction

Electric thrusters have been widely adopted for in-space propulsion applications over the past decades, with many technologies reaching high maturity levels. The decoupling of the power source from the propellant enables electric propulsion (EP) technologies to achieve fuel efficiencies much higher than those obtainable with chemical thrusters. At the same time, for a fixed amount of available power, EP units are bound to a trade-off between thrust and specific impulse (I_{sp}) [1], often resulting in very low thrust-to-power ratios (TPRs). An important class of EP technologies is that of electrothermal thrusters, which are typically characterized by moderate I_{sp} and high TPR, and are well suited for space missions which require low propellant mass fractions, but at the same time have constraints on maximum allowable transfer times. The state of the art in electrothermal propulsion is represented by arcjets and resistojets, which are both well developed technologies with extensive flight heritage. However, both of them suffer from the presence of performance or life limiting factors, namely the maximum temperature of the heating element in resistojets and the electrode erosion in arcjets.

In this framework, the Microwave Electrothermal Thruster (MET) represents an interesting novelty. The MET employs microwaves in a cilindrycal resonant cavity to ignite and sustain a plasma, which heats a gaseous propellant flowing around it [2, 3]. The hot gas is then accelerated and ejected through a converging-diverging solid nozzle, producing thrust. The swirl flow of the propellant creates a radial pressure gradient in the cavity, which keeps the plasma confined and "floating" on the cavity axis, far from the cavity walls: this allows to reach very high temperatures without direct contact with solid surfaces, thus potentially overcoming the limitations of other electrothermal thrusters. The MET was invented in the 1980s at Pennsylvania State University and Michigan State University, and has since then been developed and tested in labs at a wide range of power levels (~10 W to 30 kW) and on several propellants, including hydrogen, helium, argon, xenon, nitrogen, nitrous oxide, ammonia, and water vapor [2–8]. The first MET prototypes have flown in very recent years, despite some uncertainty on the mission outcomes and the lack of scientific publications to support these tests [9].

The number of potential future applications and the success of this technology will strongly depend on the performance it can achieve, thus it is important to identify any potential performance-limiting factors and, if possible, strategies to overcome them. From a theoretical point of view, the MET is an electrothermal thruster and therefore the specific impulse should increase as the amount of power per unit propellant mass flow rate (i.e., the specific power) is increased. However, previous experimental studies have shown that, in some cases, the specific impulse does not increase monotonically, but rather reaches a peak for a certain value of the specific power, above which a performance drop occurs [2,5,10]. This is thought to possibly be due to plasma volume expansion and heat losses to the cavity walls, as well as to decrements in the coupling efficiency, although it is not completely understood if and to what extent these are the causes. Furthermore, it has not yet been observed systematically how this decrease in efficiency depends on different design parameters such as the propellant selection, chamber size, microwave frequency, and nozzle geometry,

DOI: 10.13009/EUCASS2025-586

and on the interplay between them.
Another aspect which is crucial in determining the thruster performance is the gas dynamic expansion in the nozzle, as it is responsible for the propellant exit velocity and thus the specific impulse. Most studies to date have treated the expansion using the assumption of an adiabatic and chemically frozen flow. While the latter hypothesis has been shown to be admissible [11] in first approximation, the former is not supported by data and has not been sufficiently investigated. In fact, preliminary studies [11] have indicated that thermal losses to the nozzle walls are likely to be non-negligible because of the small dimensions and high temperatures involved.
This study aims at understanding to which extent factors such as heat losses to the chamber and nozzle walls and variation of the coupling efficiency can limit the MET performance, as well as how their effects depend upon design parameters such as the chamber and nozzle size, propellant selection, and the operating frequency. Theoretical models of the MET capable of capturing these effects are developed, and parametric numerical simulations are performed over a wide range of operating conditions, allowing for a better sensitivity on the obtained results.

2. Figures of merit

There are different quantities which we use in this work to evaluate the thruster performance across the range of previously mentioned conditions. The specific impulse is evaluated neglecting the static contribution of the nozzle [1], assuming it is small, and thus is computed as:

$$I_{sp} \approx \frac{v_{ex}}{g_0} \tag{1}$$

where v_{ex} is the propellant velocity at the nozzle exit, and g_0 is the standard acceleration due to to gravity on Earth at sea level.
The other main figures of merit are related to power flow and dissipation processes in the MET, which can be seen in Fig.1. When a certain amount of forward input power (P_{in}) is delivered to the thruster, part of it is absorbed (P_{abs}) and part of it is reflected (P_{ref}) by the plasma. We define the coupling efficiency (η_{coup}) as the ratio between absorbed and input power, namely:

$$\eta_{coup} = \frac{P_{abs}}{P_{in}} = \frac{P_{in} - P_{ref}}{P_{in}} \tag{2}$$

The absorbed power is used to heat the propellant and increase its enthalpy before it is ejected through the nozzle. However, part of it is lost as power dissipated to the cavity walls (P_{diss}) through convection, adding an infecciency to the system. It is thus useful to define the cavity dissipated power fraction (ξ_c) as the ratio between the dissipated and the absorbed power:

$$\xi_c = \frac{P_{diss}}{P_{abs}} \tag{3}$$

Similarly, in the case of a non-adiabatic expansion, power can also be dissipated through the nozzle walls and impact the thruster performance. Thereby, it is useful to define the nozzle dissipated power fraction ξ_{nozzle} as the ratio between the total enthalpy variation from nozzle inlet (h_{t_0}) to outlet ($h_{t_{ex}}$) and the total enthalpy at the nozzle inlet (see section 3.2), namely:

$$\xi_{nozzle} = \frac{\Delta h_t}{h_{t_0}} = \frac{h_{t_0} - h_{t_{ex}}}{h_{t_0}} \tag{4}$$

Finally, an important quantity is the specific power (or specific energy), defined as the ratio between the electrical input power and the propellant mass flow rate ($P_{in}/\dot{m}$). A higher specific power is generally required to increase the thrust or the I_{sp}, and can be achieved either by increasing the input power or decreasing the propellant mass flow rate.

3. Models and simulation setup

This work presents two main models used to evaluate MET performance, which are described in the following sections.
The first is a global plasma model that is used to evaluate how plasma characteristics and propellant heating in the resonant cavity depend on input power and propellant mass flow rate. This model is composed by a set of algebraic non-linear equations, which are solved numerically, and uses a simplified approach (i.e., frozen flow assumption) to treat the propellant expansion in the nozzle and estimate the exit velocity and I_{sp}.

DOI: 10.13009/EUCASS2025-586

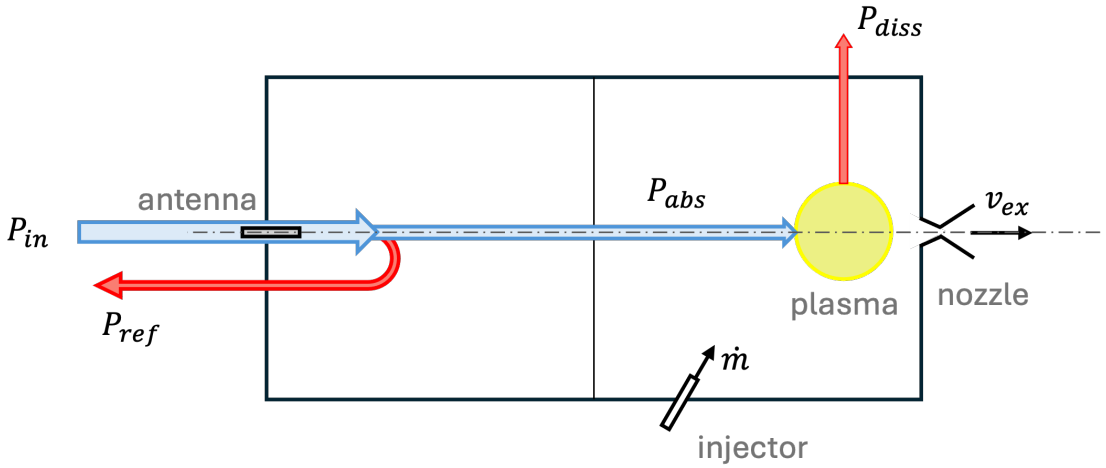

Figure 1: MET scheme and power flow.

The second is a model for the gas dynamic expansion, which allows to estimate and account for power losses to the nozzle walls self-consistently, and it is made of a set of non-linear ordinary differential equations (ODEs), also solved numerically. This model uses the chamber conditions computed by the plasma model to evaluate the nozzle inlet conditions, which are necessary to start the integration of the ODEs.

3.1 Global plasma model

The model for the resonant cavity is the same as that developed in [12] and is a global (0D) model which can compute time-dependent or steady-state, volume-averaged physical quantities. We report here a brief description of the model and the main assumptions. For a more complete description of this model, the reader is referred to [12].
The model assumes that a certain mass flow rate ($\dot{m}$) of propellant enters the resonant cavity at a reference condition and a certain amount of input electromagnetic power is applied (P_{in}). Part of this power is absorbed (P_{abs}) and part of it is reflected (P_{ref}). The relationship between input, absorbed and reflected power can be expressed using the reflection coefficient (Γ_ω), which is a quantity that depends on the plasma properties and the wave frequency, as shown below:

$$P_{abs} = P_{in} - P_{ref} = P_{in}(1 - \Gamma_\omega) \tag{5}$$

The absorbed power is partially used to energize the propellant and part of it is lost to the cavity walls either through heat exchange or through collisions. As it is heated, the propellant undergoes a transformation, by means of which its temperature is increased and the chemical composition may vary according to the possible chemical reactions (e.g., ionization, excitation, etc.). The propellant thus reaches a thermodynamic state that can be characterized by a set of physical quantities, i.e., the heavy species temperature (T_c), the electron temperature (T_e), and the number density of each species j (n_j). To determine these quantities, the model solves the steady-state of a set of particle (PaBE) and power (PoBE) balance equations [12], which are non-linear algebraic equations. The ideal gas law is then used to determine the chamber pressure p_c starting from these quantities.
In this model, neutral particles are assumed to exit the cavity by means of a choked quasi-one-dimensional, frozen, and isentropic expansion through the nozzle, which has a throat area $A^* = \pi R^{*2}$ (where R^* is the radius at the throat). Three different values of R^* ($0.175\ mm, 0.350\ mm, 0.700\ mm$) have been used, to investigate the impact of this parameter on the plasma properties in the chamber and on the exit velocity. In general, we expect that for a fixed mass flow rate, a smaller throat radius will produce a higher chamber pressure and increasing number densities. These will, in turn, affect the power absorption process in a positive or negative way, depending on the operating conditions and their impact on the reflection coefficient, and thus produce also different chamber temperatures and exit velocities.
Another important aspect is the cavity size: different cavity dimensions will lead to different plasma volumes, as well as larger or smaller surfaces over which the power loss mechanisms (i.e., convection or diffusion) may occur, thus affecting the chamber conditions. Furthermore, from electromagnetic (EM) theory it is known that the resonant frequency (f_{res}) of the TM_{011} mode at which the MET operates [13] is related to the chamber dimensions as follows:

DOI: 10.13009/EUCASS2025-586

$$f_{res} = \frac{1}{2\pi\sqrt{\mu\epsilon}}\sqrt{\left(\frac{\chi_{01}}{R_c}\right)^2 + \left(\frac{\pi}{L_c}\right)^2} \tag{6}$$

where R_c and L_c are the cavity radius and height, respectively, μ and ϵ are the permeability and permittivity of the medium in the cavity, and $\chi_{01} \approx 2.405$. Increasing the chamber dimensions will lower the resonant frequency, and vice versa. As mentioned previously, the reflection coefficient Γ_ω depends, among others, on the frequency of the EM wave, meaning that chamber dimensions can have an impact on the power absorption process and thus on the thruster performance. In this work, we considered two cavity sizes with similar aspect ratio ($AR = L_c/R_c$) and different resonant frequency, whose size is comparable to that found in [14] and [15]. The corresponding data is reported in Table 1.

Table 1: Considered cavity dimensions and corresponding wave frequency.

R_c [mm]	L_c [mm]	AR [-]	f_{res} [GHz]
50	175	3.5	2.45
16	51.5	3.2	7.50

3.2 Non-adiabatic nozzle expansion model

The following sections describe the model developed for the gas dynamic expansion of the propellant in the nozzle, assuming that it may exchange heat with the nozzle walls. This model, based on the Euler equations, requires a point-wise definition of the nozzle geometry and modeling of the heat exchange between the gas and the solid walls, which are also shown below. The model is applied to helium in this case, but it is developed and is valid for any ideal monoatomic gas.

3.2.1 Nozzle geometry

The nozzle used for simulations in this work is a converging-diverging conical nozzle, with a cone half-angle (θ) of 15°. The nozzle expansion ratio, defined as the ratio between the cross-sectional area at a generic point (A) and that at the throat (A^*) can be related to the nozzle axial coordinate x through equation (7).

$$\frac{A}{A^*} = 1 + \left(\frac{\theta x}{R^*}\right)^2 \tag{7}$$

where $x = 0$ corresponds to the throat section and to the respective radius (R^*) and area ($A^* = \pi R^{*2}$). Coordinate positive verse corresponds to the one of the expanding flow, i.e., from resonant cavity towards the exit. The x coordinate corresponding to a given expansion ratio is obtained by inverting relation (3) and taking the negative or positive value of x if the point is in the converging or diverging section of the nozzle, respectively. The nozzle radius (R) at a generic point is simply $R = \sqrt{A/\pi}$. Two different values of the throat diameter, namely 0.7 *mm* and 0.35 *mm*, have been used to investigate the performance dependency on this parameter.

3.2.2 Flow description

The model for the gas dynamic expansion is derived starting from the steady state form of the quasi-1D Euler equations [16] for a non-reacting monoatomic gas. To account for non-adiabaticity effects (i.e., heat transfer from or to the nozzle walls) a source term has been included in the energy equation. The resulting system is reported in Eq. (8):

$$\begin{cases} \dfrac{d(\rho v A)}{dx} = 0 \\ \rho v \dfrac{dv}{dx} = -\dfrac{dp}{dx} \\ \dfrac{dh}{dx} = -v\dfrac{dv}{dx} + \dfrac{\delta q}{dx} \end{cases} \tag{8}$$

where ρ is the gas density, v is the axial velocity, p is the gas pressure, h is the specific enthalpy per unit mass, x is the axial coordinate, and A is the nozzle cross-sectional area, which is a known function of the axial coordinate through

DOI: 10.13009/EUCASS2025-586

equation (3). The quantity δq represents the variation in the total specific enthalpy (h_t) due to heat transfer with the nozzle walls, as shown in Eq. (9), and is positive for heat entering the gas and negative for heat exiting the gas.

$$\delta q = dh_t = d\left(h + \frac{v^2}{2}\right) \tag{9}$$

The specific enthalpy for a monoatomic gas (species A) can be rewritten introducing the temperature gas T as:

$$h = \frac{5}{2}\mathcal{R}_A T \tag{10}$$

where $\mathcal{R}_A = \mathfrak{R}_{univ}/\mathcal{M}_A$ is the gas constant of species A. The quantity $\mathcal{M}_A$ is the molar mass (in $kg\,mol^{-1}$) of species A, and $\mathfrak{R}_{univ}$ is the universal gas constant (for calculations in this work $\mathfrak{R} = 8.3145\,JK^{-1}mol^{-1}$). The ideal gas law (Eq. (11)) is used to model the pressure as function of density and temperature:

$$p = \rho \mathcal{R}_A T \tag{11}$$

We introduce the Mach number as the ratio:

$$M = \frac{v}{a} = \frac{v}{\sqrt{\gamma \mathcal{R}_A T}} \tag{12}$$

where $a = \sqrt{\gamma \mathcal{R}_A T}$ is the local speed of sound and γ is the specific heat ratio of species A (for ideal monoatomic gases, $\gamma = 5/3$).
Combining all previous equations, and introducing the total temperature (T_t) such that $h_t = \frac{5}{2}\mathcal{R}_A T_t$, we can recast the system of equations (8) as a system of two ODEs in the variables M and T_t, namely:

$$\begin{cases} \dfrac{dM}{dx} = \dfrac{M}{1-M^2}\left(1 + \dfrac{\gamma-1}{2}M^2\right)\left[\dfrac{d\ln A}{dx} + \dfrac{1+\gamma M^2}{2}\dfrac{1}{T_t}\dfrac{dT_t}{dx}\right] \\ \dfrac{dT_t}{dx} = \dfrac{\gamma-1}{\gamma \mathcal{R}_A}\dfrac{\delta q}{dx} \end{cases} \tag{13}$$

The initial values of the state variables (i.e., M_0 and T_{t0}, corresponding to the values at the nozzle inlet) are computed starting from the chamber values of pressure (p_c) and temperature (T_c) obtained with the global plasma model. Applying the continuity equation, the chamber Mach number (M_c) is obtained:

$$M_c = \frac{\dot{m}}{p_c A_c}\sqrt{\frac{\mathcal{R}_A T_c}{\gamma}} \tag{14}$$

where $\dot{m}$ is the propellant mass flow rate and A_c is the chamber cross-sectional area. The nozzle inlet Mach number is computed by applying the conservation of mass and total enthalpy between chamber and nozzle inlet, and solving the following equation [1]:

$$\frac{A_0}{A_c} = \frac{M_c}{M_0}\left(\frac{1 + \frac{\gamma-1}{2}M_c^2}{1 + \frac{\gamma-1}{2}M_0^2}\right)^{\frac{\gamma+1}{2-2\gamma}} \tag{15}$$

where A_0 is the nozzle inlet cross sectional area. The nozzle inlet total temperature is set equal to that in the chamber (T_{tc}), and is computed as:

$$T_{t0} = T_{tc} = T_c\left(1 + \frac{\gamma-1}{2}M_c^2\right) \tag{16}$$

An expression for $\delta q/dx$, needed to solve system (19), is derived in section 3.2.3. As will be shown, such expression depends on the local value of the gas temperature T. Thus, when solving the ODE system, it is necessary at each step to compute, in addition to the state variables, also the value of T. This can be easily done using the relation:

$$T = \frac{T_t}{1 + \frac{\gamma-1}{2}M^2} \tag{17}$$

DOI: 10.13009/EUCASS2025-586

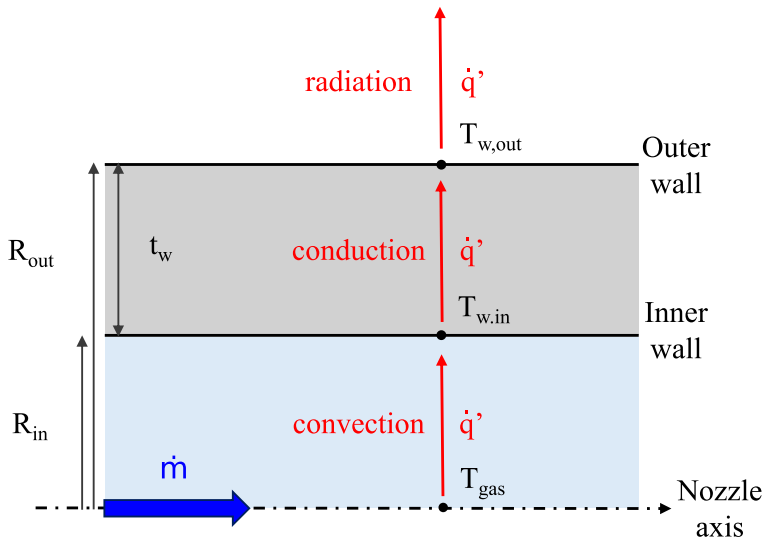

Figure 2: Heat transfer model.

3.2.3 Heat transfer model

A heat transfer model has been developed to estimate and include the power losses to the nozzle walls self-consistently in the expansion model. We account for heat transfer only in the radial direction, and consider convection between the gas and the internal nozzle walls, conduction within the solid domain, and radiation from the outer nozzle surface towards deep space, as seen in Fig. 2.
The resulting dissipated power per unit axial length ($\dot{q}'$) is evaluated as follows:

$$\dot{q}' = \frac{T - T_{w,in}}{\frac{1}{2\pi R_{in} h_g}} = \frac{T_{w,in} - T_{w,out}}{\frac{\ln(R_{out}/R_{in})}{2\pi\lambda_w}} = \frac{\varepsilon_w \sigma T_{w,out}^4}{\frac{1}{2\pi R_{out}}} \tag{18}$$

where $T_{w,in}$ and $T_{w,out}$ are the inner and outer wall nozzle temperatures, respectively, R_{in} and $R_{out} = R_{in} + t_w$ are the inner and outer nozzle radii, respectively, and t_w is the nozzle thickness. The quantity $\sigma \simeq 5.67 \times 10^{-8} Wm^{-2}K^{-4}$ is the Stefan-Boltzmann constant, $\lambda_w = 110\ Wm^{-1}K^{-1}$ [17] and $\varepsilon_w = 0.15$ [18] are representative values used for thermal conductivity and hemispherical total emissivity at the outer surface, respectively, assuming a nozzle made of tungsten. The term h_g is the convective heat transfer coefficient, computed as:

$$h_g = \frac{Nu}{2\lambda_{gas} R_{in}} \tag{19}$$

where $Nu = 3.66$ is the Nusselt number assuming a fully developed laminar flow in a duct [19], and λ_{gas} is the thermal conductivity of the gas, which is a function of the gas temperature and is computed as in [20].
The dissipated power per unit length is finally related to the total specific enthalpy variation term introduced in section 3.2.1 through the following relation:

$$\frac{\delta q}{dx} = -\frac{\dot{q}'}{\dot{m}} \tag{20}$$

4. Results and discussion

4.1 Global model results

Figures 3 to 5 show the specific impulse, coupling efficiency and cavity dissipated power fraction computed using the global plasma model as a function of the specific power. The input power has been fixed to 1000 W and the mass flow rate has been varied in order to obtain specific power values ranging from 1 MJ/kg to 100 MJ/kg. Curves are reported for both helium and argon gases, for the two operating frequencies reported in Table 1, and for the three nozzle throat radii mentioned in section 3.1.
In the case of argon, a peak in the I_{sp} is clearly present for specific power values around 5-10 MJ/kg, regardless of the operating frequency and throat size. A similar behavior is also present in the case of helium, although less pronounced

DOI: 10.13009/EUCASS2025-586

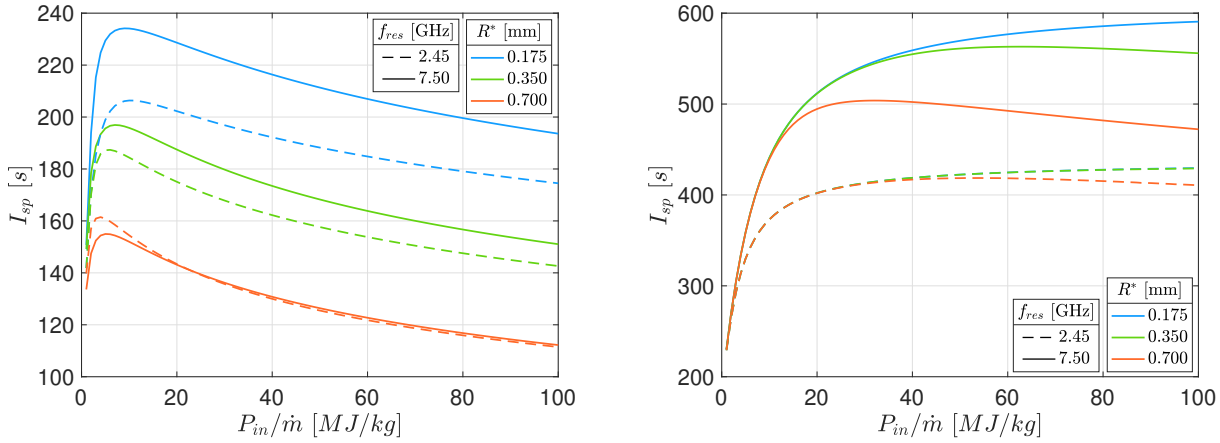

(a) Argon (b) Helium

Figure 3: Specific impulse as a function of the specific power for different propellants, microwave frequencies and nozzle throat radii. Input power $P_{in} = 1000\ W$.

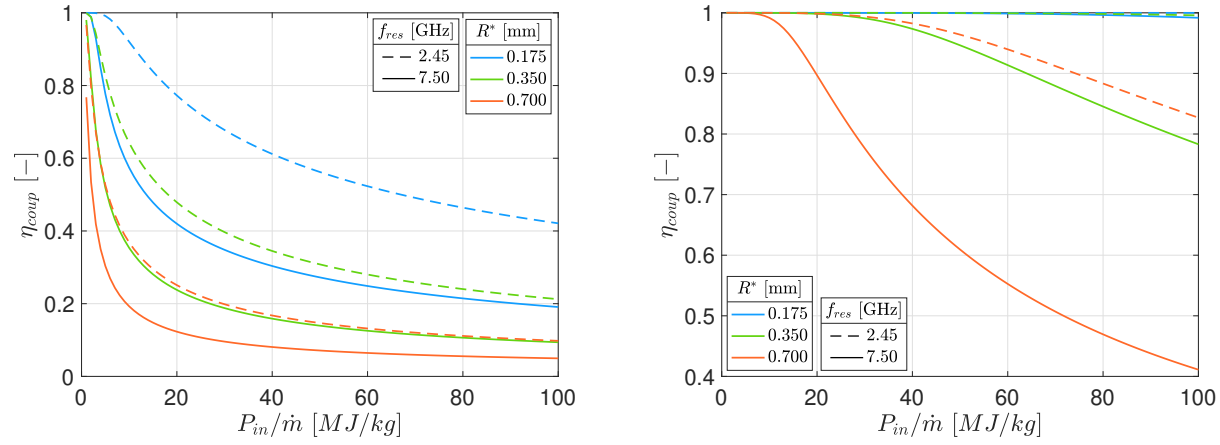

(a) Argon (b) Helium

Figure 4: Coupling efficiency as a function of the specific power for different propellants, microwave frequencies and nozzle throat radii. Input power $P_{in} = 1000\ W$.

DOI: 10.13009/EUCASS2025-586

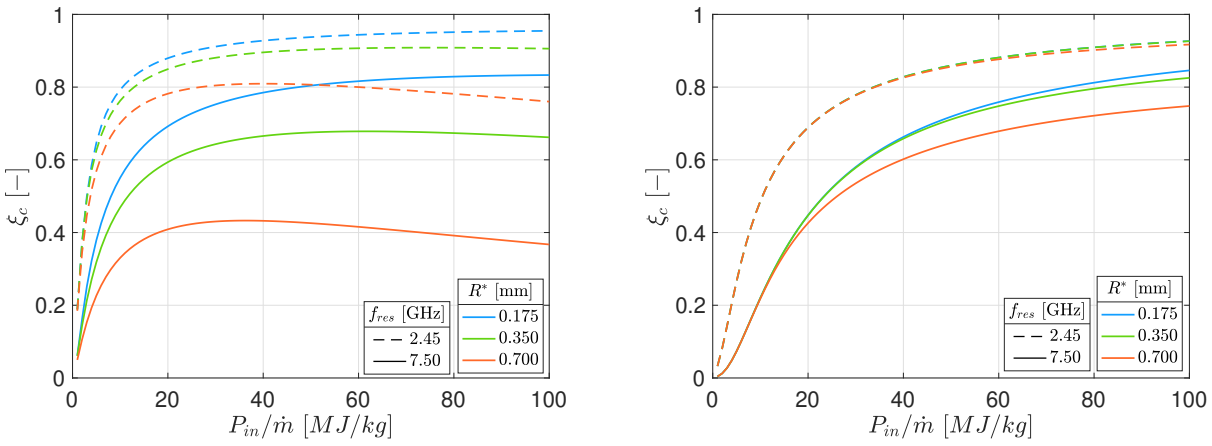

(a) Argon

(b) Helium

Figure 5: Cavity dissipated power fraction as a function of the specific power for different propellants, microwave frequencies and nozzle throat radii. Input power $P_{in} = 1000\ W$.

and only visible in the considered range for some throat radii and frequencies.
For both propellants, as seen in Fig. 3, smaller throat radii produce higher specific impulses, and the gap between curves at different values of R^* increases with increasing specific power. It appears that this difference is more pronounced in the case of the 7.50 GHz MET than in the 2.45 GHz one.
On the other hand, microwave frequency does not have a clear impact on the I_{sp}: although in most conditions it seems that a higher frequency produces a higher specific impulse, one can see how, e.g., in the case of argon for R^* of 0.700 mm the two curves at different frequency almost overlap, and the 2.45 GHz one is even slightly higher at the low specific energies.
These results can be explained observing the trends for coupling efficiency and power dissipated in the chamber in Fig.s 4 and 5. The coupling efficiency tends to decrease with increasing specific power: since the input power is fixed, an increasing specific power corresponds to a decreasing propellant mass flow rate, a lower cavity pressure and lower number densities, which ultimately reduce the plasma ability to absorb power and thus yield a higher reflection coefficient. At the same time, an increase in the specific power means more energy is available per unit mass flow rate of propellant, thus leading to higher temperatures and increased thermal losses to the cavity walls. The combined effect of decreasing coupling efficiency and increasing thermal losses result in an overall efficiency drop, which produces the undesirable peak and following drop in the I_{sp}.
The differences between the considered frequencies and throat radii are also explained as results of combinations of the coupling efficiency and wall thermal losses. Decreasing throat radii lead to higher chamber pressures and densities, which explain the higher values of η_{coup} seen for the 0.175 mm nozzle. However, more absorbed power means higher cavity temperatures and thus higher power losses to the walls, explaining the increasing values of ξ_c for decreasing R^*. Overall, the combined effect is that (for a fixed operating frequency), smaller throat radii improve the performance. Looking at the microwave frequency, on the other hand, we see that the MET operating at a lower frequency has a higher η_{coup}, At the same time, the size of the 2.45 GHz MET is much larger than the 7.50 GHz one, meaning that it has a larger surface across which power is dissipated, resulting in higher thermal losses and increased ξ_c. It appears that this last effect is in most cases more dominant, leading to a net lower performance of the 2.45 GHz MET. However, as already pointed out, this is not always the case, as seen for example for argon at the low specific energies and the 0.700 mm nozzle.
One final remark concerns the difference between the two propellants: although the behavior is not too different, it clearly appears how variations in the η_{coup} and ξ_c happen over much broader ranges of the specific power for helium compared to argon. We expect that this can be due to the higher specific heat of helium, which means that the same increase in the specific power will lead to less pronounced temperature variations and consequently also in the other physical quantities responsible for reflections and thermal losses.

4.2 Non-adiabatic expansion results

Fig. 6 displays the results obtained using the non-adiabatic gas dynamic expansion model presented in section 3.2 for the 2.45 GHz MET operating on helium propellant over a specific power range from 1 MJ/kg to 100 MJ/kg. Two values

DOI: 10.13009/EUCASS2025-586

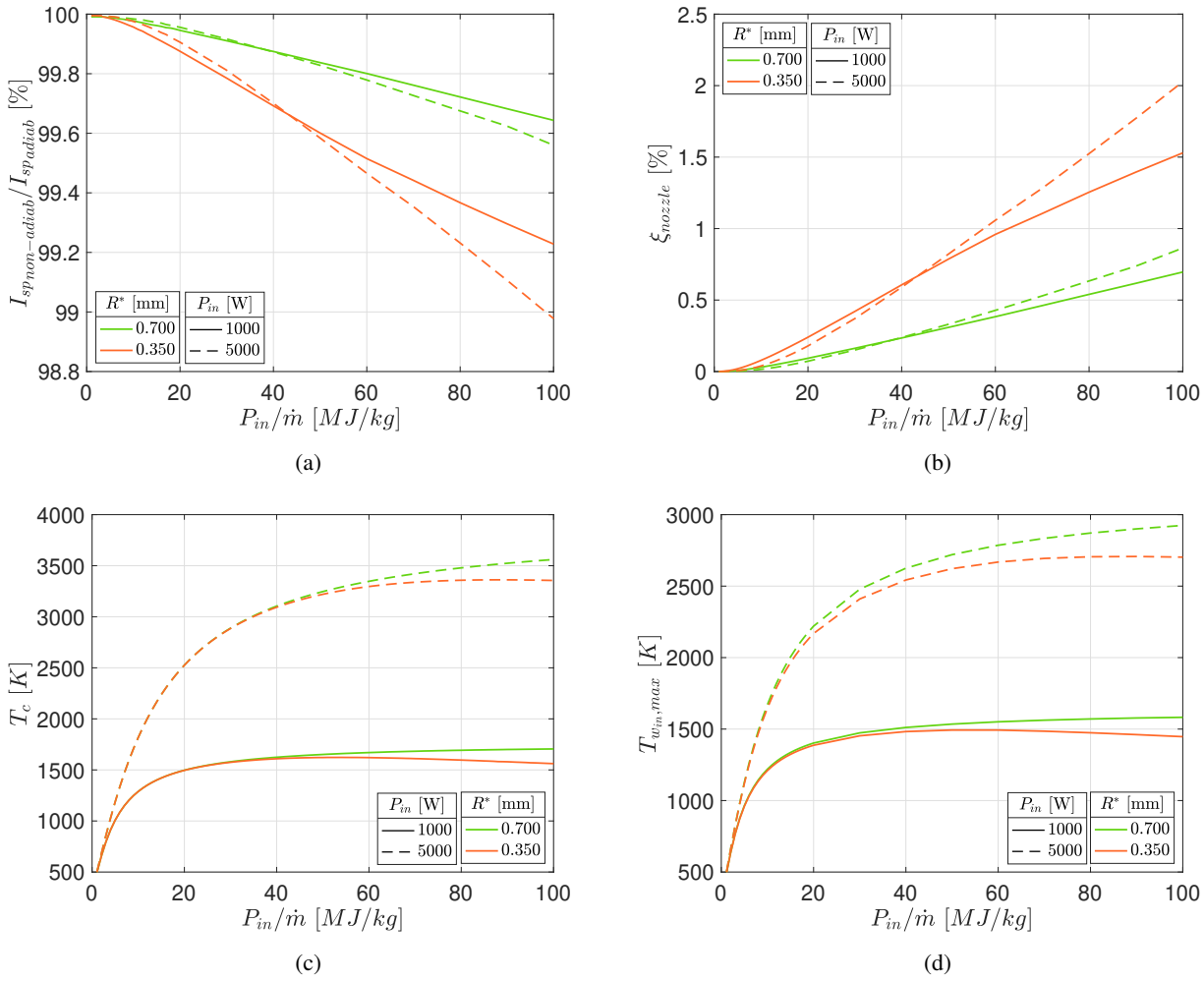

Figure 6: Ratio between I_{sp} for a non-adiabatic and adiabatic expansion (a), nozzle dissipated power fraction (b), chamber heavy species temperature (c) and maximum inner wall temperature (d) as functions of the specific power for a helium gas, different values of input power and throat radii (f_{res} = 2.45 GHz).

of the throat radius (0.700 mm and 0.350 mm) and two values of the input power (1000 W and 5000 W) have been considered in all simulations.

As can be seen in Fig. 6a, the non-adiabaticity of the nozzle expansion has little impact on the specific impulse, which is reduced of less than 1% compared to the perfectly adiabatic case in the considered conditions. This is in line with the relatively low dissipated power in the nozzle, which amounts to at most 2% of the initial total enthalpy, as seen in Fig. 6b. Although this low impact of nozzle thermal losses seems in contrast to what was expected at the beginning of this paper and with other results present in the literature [11], it must be underlined that the cavity temperatures (Fig. 6c) we are dealing with here are at most about 1600 K and 3500 K for 1 kW and 5 kW input power, respectively, and are much lower than those considered for example in [11]. The corresponding maximum wall temperatures (Fig. 6d), typically obtained somewhere close to the nozzle throat, are also lower. Considering that radiative heat losses increase with the fourth power of the outer surface temperature (Eq. (18)), it can be expected that as the cavity and wall temperatures increase above 4000-5000 K, the impact of wall heat losses will become much more significant. This would be, for example, the case for argon propellant at some values of the considered specific power range. This aspect also highlights the importance of using low molecular mass propellants for future MET operation, which allow to obtain high exit velocities with lower chamber temperatures and thus lower power dissipation through the nozzle walls. Furthermore, the emissivity of the material at the outer nozzle surface has been fixed to 0.15, which is a relatively low value and contributes to the low heat dissipation, although it may increase as the material temperature rises.

The plots in Fig. 6 clearly indicate that operation at higher power will lead on one side to higher temperatures (and this is beneficial, as it translates into a higher I_{sp}), but also, inevitably, to higher nozzle power dissipation. It also appears from the results that a larger nozzle throat is beneficial from this point of view: the performance of the 0.700 mm

DOI: 10.13009/EUCASS2025-586

nozzle is consistently better than that of the 0.350 mm one, and the nozzle dissipated power fraction of the former is about half of the latter.

5. Conclusions

This study has presented parametric simulations of the Microwave Electrothermal Thruster operating on monoatomic propellants (i.e., argon and helium). The simulations have been performed exploiting a recently developed global plasma model for the resonant cavity and a non-adiabatic model for the gas dynamic expansion based on the Euler equations. The effects of design parameters (i.e., microwave frequency and nozzle throat variation) and thermal losses to the nozzle walls on performance have been investigated.
Using the global plasma model, it was observed that power reflections and dissipation to the cavity walls represent large inefficiencies which explain the presence of a peak I_{sp} corresponding to a given value of the specific power. The computed I_{sp} is the result of a combination of these two effects, which are coupled together and have different dependencies on the afore-mentioned design parameters. In general, it was observed that smaller throat dimensions and higher operating frequency produce higher specific impulses for both propellants in most conditions, although a few exceptions exist in the considered specific power range.
Applying the non-adiabatic expansion model to helium it was seen that heat losses to the nozzle walls are small ($< 1\%$ reduction in the I_{sp}) at the considered conditions, although this is probably due to the low cavity temperatures found for helium as well as the low emissivity of the considered nozzle material.
The present work has clearly shown the importance of reflections and heat losses to the thruster walls, and future efforts shall be made to refine the assumptions used for modeling of these effects. The same approach presented here may also be applied, with appropriate modifications, to other propellants of interest for future MET applications (e.g., H_2O).

6. Acknowledgements

The authors wish to thank D-Orbit S.p.A. in the persons of D. Zuin and A. Conte for their support and suggestions in the development of this research.

References

[1] G. P. Sutton and O. Biblarz. *Rocket Propulsion Elements*. John Wiley and Sons, Inc., New Jersey, ninth edition, 2017.

[2] K. D. Diamant, B. L. Zeigler, and R. B. Cohen. Microwave electrothermal thruster performance. *Journal of Propulsion and Power*, 23(1):27–34, 2007.

[3] M. M. Micci, S. G. Bilén, and D. E. Clemens. History and current status of the microwave electrothermal thruster. In Array, editor, *EUCASS Proceedings Series – Advances in AeroSpace Sciences*, volume 1, pages 425–438, 2009.

[4] J.L. Power. Microwave electrothermal propulsion for space. *IEEE Transactions on Microwave Theory and Techniques*, 40(6):1179–1191, 1992.

[5] J.E. Brandenburg, J. Kline, and D. Sullivan. The microwave electro-thermal (met) thruster using water vapor propellant. *IEEE Transactions on Plasma Science*, 33(2):776–782, 2005.

[6] M. S. Yildiz, U. Kokal, and M. Celik. Preliminary thrust measurement results of the bustlab microwave electrothermal thruster. *53rd AIAA/SAE/ASEE Joint Propulsion Conference*, 2017.

[7] D. Staab, S. Reeve, T. Baxter, H. Lekuona, H. Larsen, H. Longhi, K. Swar, A. Garbayo, and C. Ryan. (x)met: design and test of microwave electrothermal thrusters with argon and xenon. In *Space Propulsion Conference 2020/21*, March 2021.

[8] S. Biswas, M. Beckerle, J. Mcternan, and S. Bilén. Thrust measurements of a 17.8-ghz ammonia microwave electrothermal thruster for small satellites. In *37th International Electric Propulsion Conference, Massachusetts Institute of Technology, Cambridge, MA, USA*, 06 2022.

[9] Momentus Inc. Missions. `https://investors.momentus.space/news-releases/news-release-details/momentus-new-spacecraft-engine-continues-successful-space/`. Accessed: 6 February 2025.

DOI: 10.13009/EUCASS2025-586

[10] D. Clemens, M. Micci, S. Bilén, J. Hopkins, J. Blum, C. DeForce, and S. Chianese. Evaluation and optimization of an 8-ghz microwave electrothermal thruster. In *46th AIAA/ASME/SAE/ASEE Joint Propulsion Conference & Exhibit*, 2010.

[11] M. Nava, F. Maggi, and D. Zuin. Gasdynamic expansion models and preliminary heat transfer and thermal analysis for the nozzle of a microwave electrothermal thruster using different propellants, 2024. Paper presented at the 75th International Astronautical Congress, Milan, Italy, 14–18 October.

[12] M. Lauriola, M. Nava, A. Maffini, F. Maggi, and M. Passoni. Global plasma modeling of an argon and helium fed microwave electrothermal thruster operating at kilowatts power levels. In *EUCASS Proceedings Series – Advances in AeroSpace Sciences*, 2025.

[13] D. E. Clemens. Performance evaluation of the microwave electrothermal thruster using nitrogen, simulated hydrazine and ammonia, 2008. PhD Thesis, The Pennsylvania State University.

[14] M. S. Yildiz and M. Celik. Global energy transfer model of a microwave electrothermal thruster operating with helium propellant at 2.45-ghz frequency. *IEEE Transactions on Plasma Science*, 45(8):2314–2322, 2017.

[15] F. Bosi. Global model of microwave plasma assisted n_2o dissociation for monopropellant propulsion. *Physics of Plasmas*, 26(3):033510, 2019.

[16] A. H. Shapiro. *The dynamics and thermodynamics of compressible fluid flow*. Wiley, New York, first edition, 1953.

[17] Igor L. Shabalin. *Tungsten*, pages 237–315. Springer Netherlands, Dordrecht, 2014.

[18] T. Matsumoto, A. Cezairliyan, and D. Basak. Hemispherical total emissivity of niobium, molybdenum, and tungsten at high temperatures using a combined transient and brief steady-state technique. *International Journal of Thermophysics*, 20:943–952, 1999.

[19] F. Incropera and D. DeWitt. *Fundamentals of Heat and Mass Transfer*. J. Wiley & Sons, New York, 6th edition, 2007.

[20] R. A. Svehla. *Transport Coefficients for the NASA Lewis Chemical Equilibrium Program*. NASA Technical Memorandum 4647, Cleveland, OH, 1995.